

## A Laboratory Combustor for Studies of Premixed Combustion Instability

P.A. Hield<sup>1</sup> and M.J. Brear<sup>1</sup>

<sup>1</sup>Department of Mechanical and Manufacturing Engineering  
University of Melbourne, Melbourne, Victoria, 3010 AUSTRALIA

### Abstract

Instability of premixed combustors has been a problem of considerable practical importance for several decades. This instability originates from a coupling between the flame's heat release and the combustor acoustics, and is therefore often referred to as a 'thermoacoustic' instability. The excited acoustic oscillations may cause high combustor noise levels, poor combustion, increased emissions and even catastrophic combustor failure.

Experimental rigs for the study of premixed combustion instability require that careful attention be paid to the design of the combustor and acoustic components of this coupled system. Such a rig has been designed and commissioned at the University of Melbourne. This rig allows optical study of the premixed flame and is designed to approximate true axisymmetry, so that it is appropriate for the validation of 2D and 3D numerical simulations. It also features acoustically compact upstream and downstream boundaries, including a removable throat at the combustor exit. Thus, the effect of the differing acoustic boundary conditions, which are known to have a significant effect on the instability, can also be studied.

### Introduction

Thermoacoustic oscillations can occur whenever combustion takes place within a confined space. The unsteady heat release produces sound, which is reflected at the ends of the combustion chamber and then perturbs the flame, generating more unsteady heat release. A mechanism of this phenomenon was first described by Rayleigh [1], who identified the relative phase of the pressure and heat release fluctuations as the parameter determining the stability of the system. In practical applications such as gas turbine or rocket engines, the pressure fluctuations may become so intense that structural damage occurs.

Thermoacoustic oscillations have been studied extensively over several decades [2,3]. However, most studies have concentrated on combustors with acoustically open exits, with the effect of choking the combustor exit receiving less attention [4]. This is an important omission, given that many theoretical studies suggest that a choked downstream boundary condition can have a strong effect on system stability [4-6] and also that most gas turbines feature choked (or nearly choked) combustor exits.

This paper describes the design and commissioning of a rig for the study of thermoacoustic oscillations. The rig was designed in such a way that the downstream boundary condition may be either open or choked, enabling comparison of the two boundary

conditions. Such comparisons include detailed studies on the flame dynamics using optical diagnostics such as high-speed digital cameras, photomultiplier tubes and laser diagnostics, as well as analysis of the duct acoustics with unsteady pressure transducers.

### Design of the Working Section

The experimental rig is intended to demonstrate clearly the fundamental mechanisms of thermoacoustic instability, through the coupling between the combustor acoustics and the flame heat release. Therefore detailed studies of the acoustic modes and the flame dynamics should be possible. In addition the geometry of the rig was chosen to be amenable to mathematical and numerical analysis. To achieve this, an axisymmetric geometry was chosen (figure 1). The working section is a 1m length of pipe with a boundary condition imposed at either end and a flameholder located at the midpoint. The working section is made of several short lengths of standard pipe and quartz tube, which allow easy adjustment of both its length and the flameholder position.

The choice of pipe diameter (50 mm) was a trade off between the ease of viewing and measurement of the flame and the required mass flow of air and fuel. The limiting factor was the mass flow rate of air, supplied from a dedicated 60hp Sullair screw compressor. The length to diameter ratio of the working section is 20, for which one-dimensional waves can be expected.

### The Flameholder

The flameholder provides an anchoring point for the flame by creating a recirculation zone. There are two possible generic axisymmetric flameholder geometries – an annular ring protruding from the wall or a centrally located body. However, the former can lead to an inherently 3D 'precessing jet' [7] for some flow conditions, and so the latter geometry was chosen. The shape of the flameholder was chosen to be similar to a bullet, with an elliptical nose and a short straight section (see figure 2a). The length of the elliptical nose was designed to avoid separation of the flameholder boundary layer as the flow decelerates during the transition from the ellipsoidal to the cylindrical section, and the length of the straight section was kept short to ensure that the boundary layer remains laminar prior to the bluff separation.

During the initial testing of the rig, it was found that the flameholder did not support the flame for a sufficiently wide range of operating conditions. The flameholder shape was modified through a trial and error process to incorporate some features of designs in the literature (eg [8-10]). The final design incorporated a lip on the outside rim of the flameholder, which

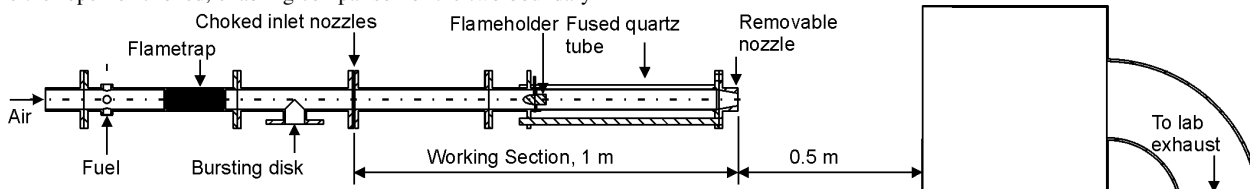


Figure 1. The rig geometry, showing the working section and the exhaust duct.

angles the flow outwards, increasing the size of the recirculation zone, and a conical indent in the downstream face (see figure 2b).

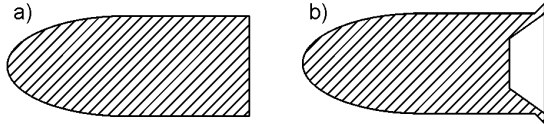


Figure 2. Cross-section view of the flameholder. a) Original design and b) modified design.

### Boundary Conditions

This study considers the effect of open and choked boundary conditions on the system stability. Previous studies by the present authors [6] using Dowling's 1995 model [11] suggest that the form of the upstream boundary condition mainly affects the frequency of the oscillations, with only a small effect on the system stability. Conversely, the form of the downstream boundary condition has a significant effect on the stability. Therefore it was decided to use a choked upstream boundary condition, but to allow for both open and choked downstream boundary conditions.

Choked inlet nozzles described in the literature (see [8]) consist of a centrally located conical 'mass flow plug' which can be moved axially inside a restriction to vary the throat area and hence the mass flow rate. However this may lead to a non-uniform flow in the working section. A new design of choked nozzle was used for the upstream boundary condition, consisting of a plate with fifteen small chamfered holes spaced evenly over the plate (figure 3). The mass flow rate is varied by controlling the stagnation pressure upstream of the nozzle. This nozzle design is approximately axisymmetric and, due to the small size of the jets produced, leads to uniform flow relatively quickly.

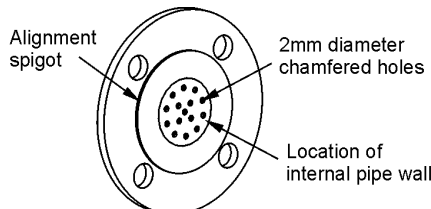


Figure 3. The choked inlet nozzle.

Marble and Candel [12] show that a choked nozzle can convert incident entropy disturbances into reflected pressure fluctuations:

$$\frac{p'}{p} = 2 \frac{u'}{u} + \frac{\rho'}{\rho} \quad (1)$$

This can have a significant destabilising effect, which has not been thoroughly experimentally investigated in the literature. Thus the rig was designed so that the downstream boundary condition can be either open or choked. This was achieved using a variety of short sections of pipe on the downstream end of the rig, which can be easily interchanged to vary the nozzle throat areas over a range of discrete values (figure 4).

### The Fuel Supply

The fuel chosen was commercial LPG, as this fuel is readily available for a reasonable cost. A gas analysis provided by the

supplier indicated that the LPG was on average 98% propane. The fuel supply system used is shown in figure 5. The propane is supplied as a vapour from three cylinders to provide a sufficient surface area for the heat transfer required to vaporise the liquid. The pressure is regulated and the mass flow rate is measured using an ABB 10A3200 armoured purgemaster volumetric flowmeter with temperature and pressure measurement on the inlet. The flow rate is controlled using two flow metering needle valves for fine control over a wide range of fuel flow rates. There is a solenoid shut off valve immediately downstream of the cylinders connected to the safety trip system, and pressure relief downstream of the regulator. Backflow of air into the fuel line is prevented using a check valve immediately before the fuel enters the main air pipe. The fuel is injected into the air pipe far enough upstream of the working section to ensure adequate mixing, and the fuel/air mixture passes through a flame trap before entering the working section (figure 1).

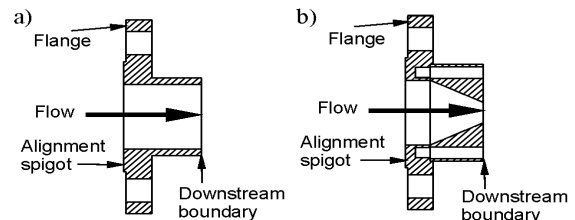


Figure 4. a) The open combustor exit and b) the choked nozzle

### Optical Access

Optical access to the working section allows the measurement of flame properties using optical techniques. The instantaneous heat release rate can be inferred from the chemiluminescence of the CH radical measured using a photomultiplier tube (PMT) and a narrow band filter centred at 431 nm [13,14].

Downstream of the flameholder to 60 mm upstream of the combustor exit, the working section is constructed from 50mm internal diameter GE 214 fused quartz tubing with 2.5mm wall thickness (figure 1). The fused quartz is held at either end in sockets in the stainless steel pipe with solastic gasket material to provide both cushioning and a seal. A stainless steel section of identical length to the glass tube can also be fitted, to allow the acoustic pressure fluctuations to be measured along the whole length of the working section.

### The Exhaust

The exhaust system must safely remove the hot exhaust gases from the test cell, while not affecting the combustor exit boundary condition. If the downstream boundary condition is choked, the exhaust pipework is acoustically isolated from the working section, but if it is open the exhaust system must replicate an infinite volume as closely as possible within the confined space of the test cell (figure 1).

The laboratory exhaust system consists of a 12" pipe running under the floor with a fan at the exit to draw air through the system. Calculations showed that the mixing of the hot exhaust from the working section with the cold air drawn through the exhaust system would be sufficient to cool the rig exhaust to an acceptable temperature.

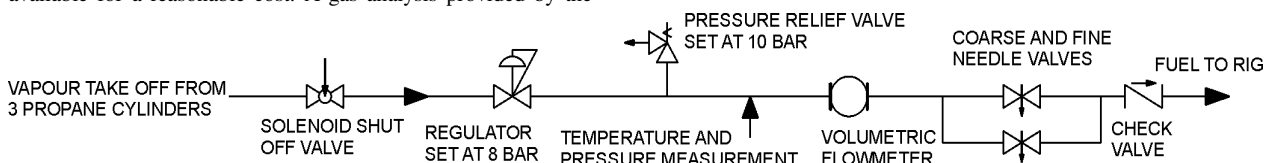


Figure 5. The fuel supply

The working section, test cell and exhaust were modelled using Matlab's PDE toolbox to solve the wave equation numerically. A numerical analogue to the two-microphone technique [15] was used to determine the reflection coefficient of the combustor exit. Incremental geometry changes were made to improve the reflection coefficient. The model assumed constant temperature and no flow over the domain, but it was expected that the trends shown in the simulation would be replicated on the experimental rig. It was found that an exhaust with an area 100 times greater than that of the working section and a gap of 0.5m between the end of the working section and the exhaust gave a reflection coefficient close to the ideal value of  $R = -1$  over the frequency range of interest (figure 6). Experimental measurements later confirmed the theoretical results [16].

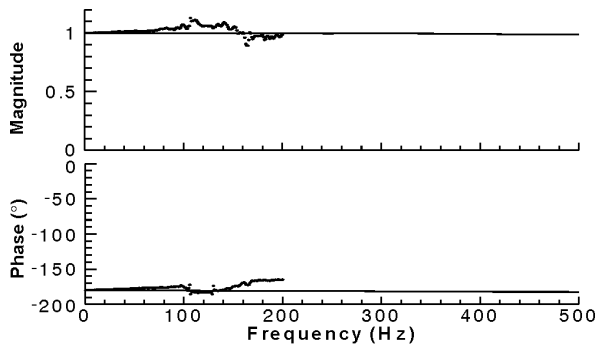


Figure 6. The simulated exhaust system reflection coefficient (solid) and the experimentally measured reflection coefficient (dots)

### Transducers

The operating point of the rig is determined by its geometry (the overall length, flameholder position and the downstream nozzle), the mean Mach number and the equivalence ratio. These parameters must be determined during operation of the rig. The choked inlet nozzle was calibrated during the commissioning of the rig (see section 3), enabling the working section mass flow rate (and hence Mach number) to be determined from measurements of the stagnation pressure at a reference position upstream of the choked inlet nozzle, the static pressure in the working section and the temperature either side of the inlet nozzle. The equivalence ratio is calculated from the total mass flow determined above and the fuel flow rate, measured using a rotameter together with pressure and temperature measurements (figure 5). The pressures were measured using Druck PTX1400 0-10 bar absolute pressure transducers, and the temperatures were measured using Temperature Controls TC39 type 'T' thermocouples with APAQ-H signal conditioning. All the steady transducers produce a 4-20 mA current output, which was passed through a resistor, and the potential drop across the resistor is recorded using a PC running LabVIEW together with a National Instruments data acquisition card.

The unsteady pressure field inside the combustor was measured using four Kulite WCT-312M water-cooled dynamic pressure transducers. One transducer was fixed as a reference at the flameholder, while the other transducers can be moved between seven ports located along the length of the working section, enabling the mode shape of the pressure field to be determined. The transducer output is recorded on the same PC as above.

### Commissioning

The rig commissioning process consisted of the testing and calibration of the equipment, as well as checking that the rig flow characteristics were acceptable. In addition, a two-stage risk assessment was performed on the rig, to ensure that the risks associated with operating the rig were acceptable. The first stage was towards the end of the design process, and identified several

modifications to improve the safety, which were then incorporated into the design. The second was during commissioning but before fuel was introduced to the rig, to confirm that the completed rig would operate as expected.

### Cold Flow Tests

The purpose of the cold flow tests was to check the uniformity of the velocity and equivalence ratio profiles in the working section, and to calibrate the rig to enable the operating condition to be measured during operation.

A pitot probe was traversed both horizontally and vertically across the working section just upstream of the flameholder at three Mach numbers, with a measurement of the dynamic pressure taken every 2 mm (figure 7). The measurements were normalised against a reference measurement to eliminate the effects of compressor 'drift'. This enabled the calculation of a normalised mass flow rate:

$$\tilde{m} = \sum_A \frac{\rho_1 u_1 A_1}{\rho_{ref} u_{ref} A} = \sum_A \sqrt{\frac{(p_t - p)_1}{(p_t - p)_{ref}}} \frac{A_1}{A}, \quad (2)$$

where  $\tilde{m}$  is the normalised mass flow rate, subscript  $1$  indicates a traverse measurement, subscript  $ref$  indicates a reference measurement,  $A_1$  is the area of the quarter-annulus corresponding to each measurement and  $A$  is the total cross section area of the duct. The density is assumed to be constant across the cross-section, and  $\tilde{m}$  is ideally independent of the mean Mach number. The normalised mass flow rate can then be used to determine the total mass flow rate (air and fuel) during operation:

$$\dot{m}_{total} = \sqrt{\frac{2p}{RT}} (p_t - p)_{ref} A \tilde{m}, \quad (3)$$

where  $p$  and  $T$  are the working section temperature and pressure, measured at the same time. The Mach number can be calculated in a similar way:

$$M = \tilde{m} \sqrt{\frac{2(p_t - p)_{ref}}{\gamma p}}. \quad (4)$$

During testing of the rig, it was found that the differential pressure transducer did not produce reliable results while the flame was present. Thus a technique for measuring the Mach number and total mass flow rate without using this transducer had to be developed. The mass flow rate through a duct can be written in terms of the stagnation properties and the Mach number:

$$\dot{m} = \frac{A p_t}{\sqrt{T_t}} \sqrt{\frac{\gamma}{R}} \left(1 + \frac{\gamma-1}{2} M^2\right)^{\frac{\gamma+1}{2(\gamma-1)}} M \quad (5)$$

(e.g. [17]). At the throat of a choked nozzle, the Mach number is unity, so the non-dimensional mass flow rate through the nozzle is constant

$$\frac{\dot{m} \sqrt{RT_t}}{A^* p_t} = \sqrt{\gamma} \left(\frac{\gamma+1}{2}\right)^{\frac{\gamma+1}{2(\gamma-1)}} = const \quad (6)$$

where  $A^*$  is the throat area. The mass flow rate through the system is constant, and the stagnation properties a short distance upstream of the throat can be assumed to be the same as those at the throat, so

$$\dot{m} \propto \frac{p_{tu}}{\sqrt{T_{tu}}}, \quad (7)$$

where the subscript  $tu$  represents stagnation conditions a short distance upstream of the inlet nozzle. Using equations (3) and (4) the working section Mach number can be related to the total mass flow rate

$$M = \frac{\dot{m}}{Ap_w} \sqrt{\frac{RT_w}{\gamma}} \quad (8)$$

where the subscript  $w$  indicates static quantities in the working section. Therefore

$$M \propto \frac{p_{tu}}{p_w} \sqrt{\frac{T_w}{T_{tu}}} \quad (9)$$

During cold flow operation, the total mass flow rate and Mach number were correlated against the groups given in equations (7) and (9) respectively, and a line of best fit calculated based on the standard equation of a straight line (the correlation for the mass flow is shown in figure 8). The total mass flow rate and Mach number were then calculated from these straight-line equations. The non-zero y-axis intercepts are due to measurement error and physical effects not included in the theory, for example the non-perfect axisymmetry of the rig.

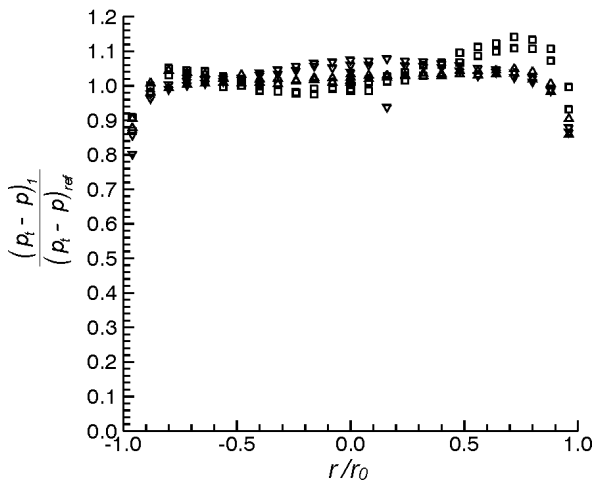


Figure 7. Profiles of the loss coefficient in the working section.  $\square$   $\bar{M} = 0.035$ ,  $\triangle$   $\bar{M} = 0.065$  and  $\nabla$   $\bar{M} = 0.090$ .

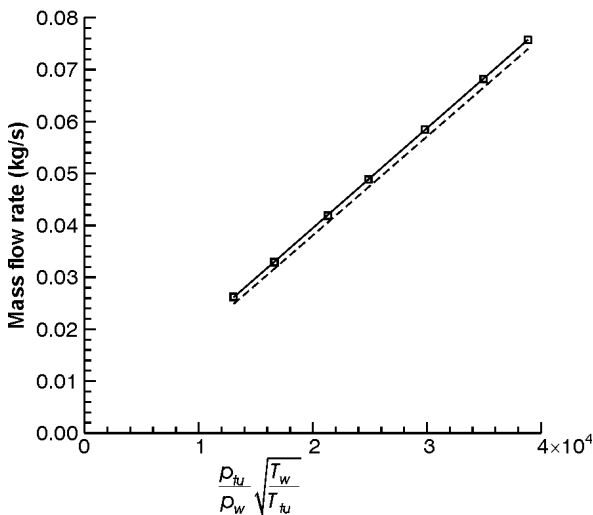


Figure 8. The total mass flow plotted against the correlation parameter. Squares: measurement, solid line: regression line and dashed line: theoretical prediction

To check the fuel-air premixing, a Combustion Fast Flame Ionisation Detector (Fast FID) probe was traversed both horizontally and vertically across the working section just upstream of the flameholder. This measurement showed that the premixed fuel and air mixture was uniform to within 5% in all but a few isolated cases. A typical traverse is shown in figure 9.

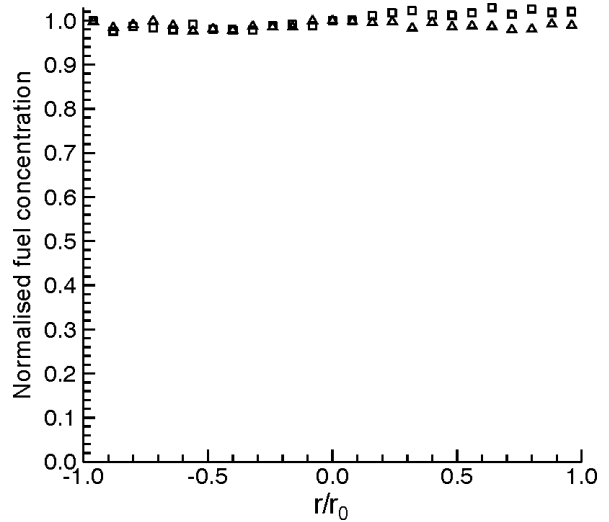


Figure 9. Profiles of equivalence ratio in the working section, in both horizontal ( $\triangle$ ) and vertical ( $\square$ ) directions

## Results

Figure 10 shows a typical limit cycle in combustor pressure. The transducer is located 40 mm downstream of the working section inlet nozzle, where the largest pressure fluctuations are expected to occur. The fundamental frequency of the duct mode is clear, and corresponds reasonably well with that predicted in the stability analysis of this geometry [6]. The amplitude of these acoustic fluctuations is substantial, and are in keeping with other studies of thermoacoustic instabilities of premixed flames in laboratory combustors [4,8].

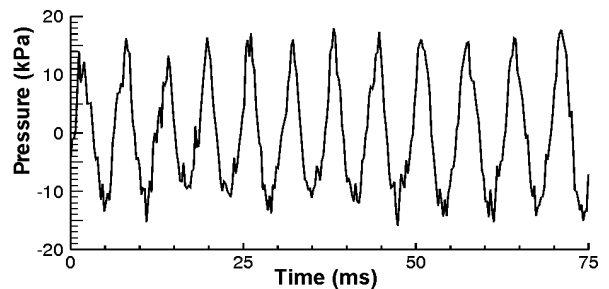


Figure 10. A typical limit cycle pressure oscillation

Thermoacoustic oscillations are driven by a coupling between the duct acoustics and fluctuations in the heat release from the flame. Optical techniques can be used to study the behaviour of the flame in response to acoustic fluctuations at the flameholder. Figure 11 shows typical flame motion over one thermoacoustic cycle. The pictures of the flame were recorded using a high-speed digital camera with a frame rate of 2000 Hz. The velocity fluctuations at the flameholder were calculated from pressure measurements [18], and are shown as a phase reference. The position of each picture in the cycle is also shown. The flame can clearly be seen to grow from a small kernel near the flameholder to fill almost the entire duct before disappearing.

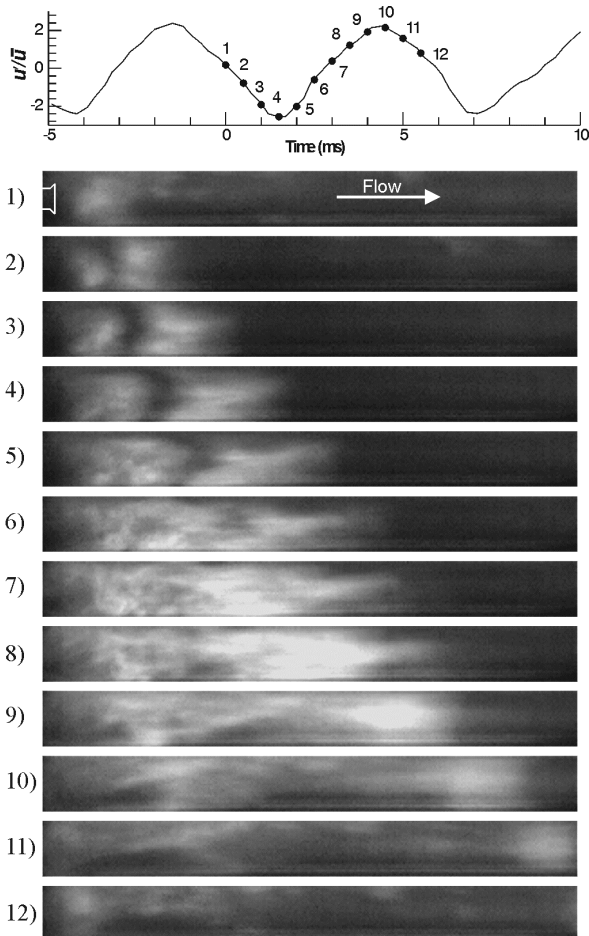


Figure 11. Fluctuations of the flame in response to fluctuations in the velocity at the flameholder. The pictures were recorded using a high-speed digital camera at 2000 Hz.

### Conclusions

A rig has been designed for the study of thermoacoustic instability of premixed combustion. It consists of an axisymmetric combustion chamber 1 m long and 50 mm in diameter, with a flameholder located on the centreline at the midpoint of the working section. The upstream boundary condition is choked, allowing easy regulation of the working section Mach number and acoustically decoupling the working section from the upstream pipework. The downstream boundary condition may be either open or choked, and the rig exhaust has been carefully designed to ensure that the reflection coefficient is as close as possible to the theoretical reflection coefficient of an open pipe.

The rig has been commissioned and tested, showing that the flow properties are within acceptable limits for the experimentation, and that the transducers and other peripheral equipment are functioning correctly. Detailed studies of the rig acoustics, the flame dynamics and their coupling are presented in [16,18].

### References

[1] Rayleigh, L., *The Theory of Sound*. Vol. 2, London: Macmillan and Co 1896.  
 [2] Culick, F.E.C., *Combustion Instabilities in Propulsion Systems*. Combustion Instabilities Driven by Thermochemical Acoustic Sources, ed. A.S. Hersh. Vol. 4, New York: AMSE 1989.

[3] Lieuwen, T., Modeling Premixed Combustion-Acoustic Wave Interactions: A Review. *J. Prop. Power*, **19**(5), 2003, 765-781.  
 [4] Macquisten, M.A. and Dowling, A.P., Low-Frequency Combustion Oscillations in a Model Afterburner. *Comb. Flam.*, **94**, 1993, 253-264.  
 [5] Dowling, A.P. *Acoustics of Unstable Flows*. in *Theroetical and Applied Mechanics*. 1997.  
 [6] Hield, P.A., Brear, M.J. and Moase, W.H. *A Parametric, Linear Stability Analysis of Thermoacoustic Oscillations*. in *2003 Australian Symposium on Combustion*. 2003. Monash University.  
 [7] Wong, C.Y., Nathan, G.J. and O'Doherty, T., The Effect of Initial Conditions on the Exit Flow from a Fluidic Precessing Jet Nozzle. *Expt. in Fluids*, **36**(1), 2004, 70-81.  
 [8] Langhorne, P.J., Reheat buzz: an acoustically coupled combustion instability. Part 1. Experiment. *Journal of Fluid Mechanics*, **193**, 1988, 417-443.  
 [9] Pan, J.C., Vangsness, M.D. and Ballal, D.R., Aerodynamics of bluff-body stabilized confined turbulent premixed flames. *J. Eng. Gas Turbine Power*, **114**, 1992, 783-789.  
 [10] Penner, S.S. and Williams, F., Recent studies on flame stabilization of premixed turbulent gases. *Appl. Mech. Rev.*, **10**(6), 1957, 229-237.  
 [11] Dowling, A.P., The Calculation of Thermoacoustic Oscillations. *J. Sound. Vib.*, **180**(4), 1995, 557-581.  
 [12] Marble, F.E. and Candel, S.M., Acoustic Disturbance from Gas Non-Uniformities Convected Through a Nozzle. *J. Sound Vib.*, **55**(2), 1977, 225-243.  
 [13] Balachandran, R., Ayoola, B.O., Kaminski, C.F., Dowling, A.P. and Mastorakos, E., Experimental investigation of the nonlinear response of turbulent premixed flames to imposed inlet velocity oscillations. *Comb. Flam.*, **143**(1-2), 2005, 37-55.  
 [14] Chaparro, A., Landry, E. and Cetegen, B.M., Transfer function characteristics of bluff-body stabilized, conical V-shaped premixed turbulent propane-air flames. *Comb. Flam.*, **145**(1-2), 2006, 290-299.  
 [15] Seybert, A.F. and Ross, D.F., Experimental Determination of Acoustic Properties using a Two-Microphone Random-Excitation Technique. *J. Acoust. Soc. Am.*, **61**(5), 1977, 1362-1370.  
 [16] Hield, P.A. and Brear, M.J. *A comparison of open and choked exits of a premixed combustor during thermoacoustic limit cycle*. in *13th AIAA/CEAS Aeoaoustics Conference*. 2007. Rome, Italy.  
 [17] Oates, G.C., *Aerothermodynamics of Gas Turbine and Rocket Propulsion*: American Institute of Aeronautics and Astronautics, Inc 1984.  
 [18] Hield, P.A., *An experimental and theoretical study of thermoacoustic instability in a premixed turbulent laboratory combustor*: PhD Thesis, University of Melbourne 2007.